Teleconnected Influence of North Atlantic Sea Surface Temperature on the El Niño Onset

Xin Wang[1,3], Chunzai Wang[2], Wen Zhou[3], Dongxiao Wang[1*], Jie Song[4]

[1] *Key Laboratory of Tropical Marine Environmental Dynamics, South China Sea Institute of Oceanology, Chinese Academy of Sciences, Guangzhou 510301, China*

[2] *NOAA/Atlantic Oceanographic and Meteorological Laboratory, Miami, Florida, U. S. A.*

[3] *Guy Carpenter Asia-Pacific Climate Impact Centre, City University of Hong Kong, Hong Kong, China*

[4]*LASG, Institute of Atmospheric Physics, Chinese Academy of Sciences, Beijing, 100029, China*

Submitted to *Climate Dynamics*

2009

* Corresponding author:
Dr. Dongxiao Wang
Key Laboratory of Tropical Marine Environmental Dynamics
South China Sea Institute of Oceanology, Chinese Academy of Sciences
164 West Xingang Road, Guangzhou 510301, China
Phone: (86)20-8902-3204; Fax: (86)20-8902-3205
E-mail: dxwang@scsio.ac.cn

Abstract

Influence of North Atlantic sea surface temperature (SST) anomalies on tropical Pacific SST anomalies is examined. Both summer and winter North Atlantic SST anomalies are negatively related to central-eastern tropical Pacific SST anomalies in the subsequent months varying from 5-13 months. In particular, when the North Atlantic is colder than normal in the summer, an El Niño event is likely to be initiated in the subsequent spring in the tropical Pacific.

Associated with summer cold North Atlantic SST anomalies is an anomalous cyclonic circulation at low-level over the North Atlantic from subsequent October to April. Corresponded to this local response, an SST-induced heating over the North Atlantic produces a teleconncted pattern, similar to the East Atlantic/West Russia teleconnection. The pattern features two anticyclonic circulations near England and Lake Baikal, and two cyclonic circulations over the North Atlantic and near the Caspian Sea. The anticyclonic circulation near Lake Baikal enhances the continent northerlies, and strengthens the East-Asian winter monsoon. These are also associated with an off-equatorial cyclonic circulation in the western Pacific during the subsequent winter and spring, which produces equatorial westerly wind anomalies in the western Pacific. The equatorial westerly wind anomalies in the winter and spring can help initiate a Pacific El Niño event following a cold North Atlantic in the summer.

1. Introduction

El Niño-Southern Oscillation (ENSO) is the largest climate phenomenon on Earth (e.g., Wallace and Gutzler 1981; Wang et al. 2000; Wang and Zhang 2002; Li et al. 2007) and it has motivated and attracted many studies during the past decades. Some of studies focused on the western Pacific since it is believed that ENSO events are initiated in this region. For example, a westerly wind burst in the western tropical Pacific, which can excite equatorial Kelvin waves, is known to trigger El Niño outbreaks (e.g., Wyrtki 1975; Rasmusson and Carpenter 1982; Luther et al. 1983; Barnett, 1983; Huang et al. 1998; Wang and An 2002; Clarke and Shu, 2000). Many studies have also identified an important role of the western Pacific wind in the ENSO transition (Weisberg and Wang 1997a, b; McPhaden et al. 1999; Wang et al. 1999; Clarke and Van Gorder 2001). The tropical Pacific Ocean-atmosphere interaction (Weisberg and Wang 1997a, b; Wang et al. 1999; Wang and Weisberg 2000), the mid-latitude atmospheric (Chu 1988; Li 1990, 1995; Xu and Chan 2001; Li et al. 2005) and oceanic variability (Kug and Kang 2006, Xie et al. 2002; Misra 2004; Zhang and Delworth 2005; Dong et al. 2006) may all influence zonal wind anomalies in the western Pacific.

Variability of the East-Asian Winter Monsoon (EAWM) can also influence the wind anomalies in the western Pacific (Chu 1988; Chu and Frederick 1990; Li 1990, 1995; Xu and Chan 2001; Li et al. 2005). Li (1990, 1995) suggested that the frequent activity of stronger East-Asian troughs (or cold surges) in the winter can weaken the trade wind and enhance the cumulus convections over the western-central tropical

Pacific. Both Kelvin waves resulting from a reduction of the trade wind and intraseasonal oscillations caused by the stronger convection can excite El Niño events. Li et al. (2005) further suggested that an east-west pressure gradient resulting from a stronger EAWM can excite the westerly wind anomalies over the western tropical Pacific.

The results such as those shown by Gong et al. (2001), Wu and Wang (2002), Wang et al. (2005) and Lu et al. (2007) have suggested that EAWM variability may link to the Arctic Oscillation (AO) or the North Atlantic Oscillation (NAO) through the Siberian high. In addition, some studies have shown that the Northern Annular Mode (NAM) or the AO or NAO can impact tropical variability (e.g., Thompson and Lorenz 2004; Nakamura et al. 2006). However, the direct relationships between these teleconnected patterns and ENSO require further clarity.

Previous studies show a significant relationship of the SST variations over the North Atlantic with the AO or the NAO on interannual to multidecadal timescales (Latif et al. 2000; Rodwell et al. 1999). Over the twentieth century, North Atlantic SST anomalies exhibited prominent multidecadal variations (Kushnir 1994; Mann and Park 1994; Enfield et al. 2001), which can impact global climate, especially the Pacific climate, and thus be an important driver of global decadal variability (e.g., Knight et al. 2006; Sutton and Hodson 2007). These studies have shown that ENSO variability is influenced directly by Atlantic SST variability with changing the zonal wind anomalies in the Pacific via the tropical teleconnection (e.g., Dong and Sutton 2002; Zhang and Delworth 2005; Timmermann et al. 2005; Dong et al. 2006; Dong

and Sutton 2007). Using coupled general circulation models, several studies have shown that ENSO variability is related closely to changes in Atlantic SST anomalies (e.g., Dong and Sutton 2002; Zhang and Delworth 2005; Timmermann et al. 2005; Dong et al. 2006; Dong and Sutton 2007). This coupled ocean-atmosphere model results (Dong and Sutton 2002; Dong et al. 2006; Dong and Sutton 2007) have suggested that warm Atlantic SST anomalies result in a weakening of ENSO variability. The anomalous warm Atlantic SST associated with the positive phase of the Atlantic Multidecadal Oscillation (AMO) leads to changes in the mean state of the tropical Pacific, with a deepening mean thermocline and a reduction of vertical stratification of the equatorial Pacific Ocean. This remoted influence is transmitted by large-scale atmospheric circulation changes associated with anomalous diabatic heating in the tropical Atlantic. In addition to this atmospheric bridge, an oceanic teleconnection may also link the Atlantic variations with the thermocline in the tropical Pacific. Timmermann et al. (2005) suggested that a cooling in the North Atlantic associated with the weakened Atlantic thermohaline circulation leads to weakened ENSO variability and results in a suppression of ENSO variance. The difference between the studies of Timmermann et al. (2005) and Dong and Sutton (2002, 2007) is that these studies focused on the different timescales associated with oceanic and atmospheric teleconnections, respectively.

It is noted that Dong and Sutton (2002), Dong et al. (2006) and Dong and Sutton (2007) emphasized on the roles of tropical Atlantic SST anomalies in ENSO variability. Moreover, analyzing the observed data and the model results, Wang et al.

(2009) showed that North Atlantic SST anomalies are significantly related to the El Niño occurrence but not La Niña. The purpose of the present paper is to further investigate the relationship between North Atlantic SST anomalies and the El Niño onset. We show that cold North Atlantic anomalies in the summer have a teleconncted effect on the Siberian high, the EAWM and sequentially the surface wind anomalies over the western Pacific, thus affecting the El Niño onset in the tropical Pacific during the subsequent spring. These are different from the influences of tropical Atlantic SST on ENSO variability proposed by Dong and Sutton (2007) and Timmermann et al. (2005).

The paper is organized as follows. Section 2 introduces datasets and indices used in the paper. Section 3 analyzes and shows the relationship between North Atlantic SST anomalies and atmospheric and oceanic variables over the tropical Pacific. Atmospheric response to summer cold SST anomalies in the North Atlantic is presented in Section 4. A possible physical mechanism for summer cold SST anomalies in the North Atlantic to teleconnect into the tropical western Pacific is presented in Section 5. Summary and discussion are finally given in Section 6.

2. Data and indices

Datasets used in this paper include the monthly reanalysis product of the European Centre for Medium-Range Weather Forecasts (ERA40) during 1958-2001 and the monthly UK Met Office's Hadley Centre's Sea Ice and SST (HadISST) (Rayner et al. 2003) from 1870 to 2003. The variables analyzed from ERA40 include

horizontal wind, geopotential height, air temperature, wind at 10m and surface level pressure (SLP).

An ENSO index, Nino-3.4, is defined as SST anomalies averaged over the region between 5ºS-5ºN and 170ºE-120ºW. An El Niño event is defined as in Trenberth (1997). A monthly East Atlantic/West Russia (EA/WR) teleconnection index from 1950 to 2003 is provided by the National Oceanic and Atmospheric Administration's Climate Prediction Center (download from ftp://ftp.cpc.ncep.noaa.gov/wd52dg/data/indices/tele_index.nh). Midlatitude SST variability in the Atlantic is a potential forcing of overlying atmospheric variability such as the AO or NAO (Latif et al. 2000; Rodwell et al. 1999; Czaja and Frankignoul 2002). To investigate the relationship between North Atlantic SST anomalies and El Niño, we construct a North Atlantic Index (NAI) by averaging SST anomalies over the region of 30º-50ºN and 10º-50ºW. We choose this region because El Niño activity is closely related to these regional SST anomalies (Wang et al. 2009).

3. Relationship between SST anomalies in the North Atlantic and tropical Pacific

Previous studies have identified that tropical Atlantic SST anomalies can influence the ENSO event occurrence with a delayed time varying from few years to several decades (Timmermann et al. 2005; Dong and Sutton 2002, 2007; Dong et al. 2006). However, Figure 1 shows that the relationship between the monthly North Atlantic and central-eastern tropical Pacific SST anomalies during 1870-2003 varies from month to month. The significantly negative correlations occur in the boreal

summer with the Nino-3.4 index lagging the NAI by 5-13 months. This indicates that if the North Atlantic is cold in the summer, the central-eastern tropical Pacific tends to be warm in the subsequent winter, spring and summer. In addition, the significant correlations also appear in the wintertime with the Nino-3.4 index lagging the NAI by 7-13 months, suggesting that when the NAI in the winter is cold, SST anomalies in the central-eastern tropical Pacific have a tendency to be warm in the following summer, autumn and winter. The inverse relationship between the NAI and Nino-3.4 index is in agreement with the results of Wang et al. (2009) and Dong and Sutton (2002, 2007). It is noted that the lagged-correlation times between the NAI and the Nino-3.4 index are not longer than 14 months. These timescales are much shorter than those of Timmermann et al. (2005) who suggested that the connection between the North Atlantic and tropical Pacific is through oceanic processes on the timescales of many decades or longer. Therefore, our observed shorter timescales seem to suggest that an influence of North Atlantic SST anomalies on the tropical Pacific is associated with atmospheric processes instead of oceanic processes.

It is well known that El Niño is initiated in the spring (Philander, 1985). Figure 1 suggests that a cold (warm) North Atlantic in the summer can be associated with a warm (cold) tropical Pacific in the subsequent year. Table 1 exhibits the years prior to El Niño and La Niña years [denoted by El Niño(-1) La Niña(-1)] during 1958-2001. There are 13 El Niño events during the period of 1958-2001. Among these 13 events, the 10 cases are associated with a cold North Atlantic in the summer prior to El Niño year (the summer NAI is colder than 0.5 standard deviation). This indicates that a cold

summer North Atlantic is accompanied with an El Niño onset in the subsequent year. However, it is noted that the relation between the warm summer NAI and La Niña event is weak. Among the 8 La Niña events during 1958-2001, only half of them occur when the preceding summer North Atlantic is warmer (the summer NAI is warmer than 0.5 standard deviation). This poor correlation between a La Niña onset and North Atlantic SST anomalies is in agreement with our previous studies (Wang et al. 2009).

Here we examine processes that are responsible for linking cold summer SST anomalies in the North Atlantic and the subsequent El Niño onset in the tropical Pacific. Spatial patterns of lagged correlations of summer NAI with SST and surface zonal wind anomalies in the subsequent months over the tropical Pacific are shown in Figs. 2 and 3. The SST correlation shows positive correlations over the western tropical Pacific and negative correlations in the central-eastern tropical Pacific (Fig. 2). The concurrent July zonal wind (Fig. 3a) shows a negative correlation over the western tropical Pacific (140-170ºE) and a positive correlation in the eastern tropical Pacific (140-120ºW). This indicates that cold summer SST anomalies in the North Atlantic are associated with westerly wind anomalies in the western Pacific but easterly wind anomalies in the eastern Pacific. In January and April of the subsequent year, westerly wind anomalies in the western Pacific are further developed (Figs. 3c and 3d). The development of westerly wind anomalies can initiate an El Niño event by producing the downwelling oceanic Kelvin waves. In summary, our analyses suggest that a cold North Atlantic in the summer is associated with equatorial

westerly wind anomalies in the western Pacific and warm SST anomalies in the tropical Pacific during the subsequent year.

4. Atmospheric circulation associated with North Atlantic SST anomalies

Section 3 has shown that summer North Atlantic SST anomalies are related to SST and surface zonal wind anomalies over the tropical Pacific in the following year. This delayed and teleconnected influence on the tropical Pacific is on the timescales shorter than 14 months, suggesting the importance of atmospheric processes for the linkage. This section analyzes atmospheric circulation associated with North Atlantic SST changes based on the composite method.

The cold and warm years in the North Atlantic are defined when the standard deviation of the NAI exceeds 0.5. From 1958-2001, the summer NAI yields eighteen cold years and thirteen warm years. The eighteen cold years are 1958, 1962, 1963, 1964, 1966, 1968, 1969, 1970, 1971, 1974, 1978, 1981, 1982, 1984, 1985, 1992, 1993, and 1994, while the thirteen warm years are 1960, 1961, 1967, 1977, 1987, 1988, 1989, 1990, 1995, 1998, 1999, 2000, and 2001. Although the summer NAI is negative (positive) in 1963, 1969, and 1994 (1967 and 1990), they are not classified as the cold (warm) years because a La Niña (El Niño) occurs in the subsequent year from Table 1. It is noted that although the summer negative NAI is weak (less than 0.5 standard deviation) in 1975 and 1976 El Niño occurs in the following year, whereas El Niño does not occur in 1974 when the prior summer NAI is with a largest negative value. These indicate that the complex of El Niño onset, which is discussed later. To clearly

illustrate the impact of the North Atlantic on atmospheric circulations in the Pacific, cold-minus-warm composite maps are calculated from the previous year of the El Niño year to the El Niño year, which are respectively denoted by year(-1) and year(0) as in Rasmusson and Carpenter (1982).

Composite differences of zonal wind at 850-hPa between the cold and warm summer NAI from July(-1) to April(0) are shown in Fig. 4. Consistent with the correlation pattern (Fig. 3), Figure 4 shows westerly winds in the western Pacific in the following months after a cold North Atlantic in the summer. In particular, strong westerly winds appear in the western Pacific in the subsequent winter and spring (Figs. 4c and 4d). Therefore, both the correlation and composite analyses suggest that a cold summer North Atlantic can induce westerly wind anomalies over the western-central tropical Pacific in the following winter and spring, which result in eastward propagating Kelvin waves and thus trigger an El Niño in the Pacific.

Atmospheric circulations over East Asia and the western Pacific from July(-1) to April(0) are shown in Fig. 5. Overall, composite of winds features an ENSO western Pacific anomaly pattern before the El Niño onset (Wang et al. 1999; Wang and Weisberg 2000): an equatorial westerly wind anomaly in the tropical western Pacific and the associated off-equatorial cyclonic circulation in the western Pacific. In October(-1), northeasterly winds occur over the northeast of China and northwesterly winds are along the China coast (Fig. 5b). In January(0), the northerly regime shifts southward and the northwesterly system along the China coast strengthens further (Fig. 5c). However, in April(0), southerlies replace northerlies over East Asia (Fig. 5d).

It is noted that there are always northerly anomalies in the east of Philippine from the summer prior to the El Niño year to the next spring. In summary, a cold North Atlantic in the summer is associated with equatorial westerly wind anomalies in the western Pacific and northerly wind anomalies over East Asia during the subsequent winter and spring. The equatorial westerly wind anomalies are accompanied with an anomalous cyclone in the off-equatorial western Pacific, and the northerly wind anomalies over East Asia indicate a strengthening of the EAWM.

The strengthening of northerlies over East Asia after a cold summer North Atlantic is further examined by composites of the upper level wind and SLP (Figs. 6 and 7). Corresponded to the cold summer North Atlantic is an enhanced jet stream south of Japan in October(-1) and January(0) (Figs. 6b and 6c). The negative zonal wind anomalies are also located north of the jet. In this situation, the anomalous cyclonic vorticity to the north of the jet stream over East Asia enhances the cyclonic circulation and leads to the development of a trough at the lower level. This development of a trough is associated with northerly anomalies over northeastern Asia as shown in Figs. 5b and 5c (Jhun and Lee 2004). In April (0), the anomalous circulation reverses, with negative zonal wind anomalies over south of Japan and positive wind anomalies north of the negative wind anomalies. So, the anomalous anticyclonic vorticity over the East Asia region is enhanced, and it results in the anomalous anticyclonic circulation and southerlies (Fig. 5d).

Besides the jet over south of Japan, the northerlies over the East Asia relate closely to the intensity of the Siberian high. Figure 7 shows composite differences of

SLP between the cold and warm summer NAI years. It is found that significantly negative SLP anomalies are located over East Asia and the western Pacific in July(-1) (Fig. 7a). However, significantly positive SLP anomalies maintain over the region of 45º-60ºN, 90º-140ºE from October(-1) to April(0), indicating that the Siberian high is stronger in these periods following cold summer North Atlantic SST anomalies (Figs. 7b, 7c and 7d). Thus, when North Atlantic SST anomalies are cold in the summer, the Siberian high is strengthened in the following autumn, winter and spring.

5. A possible physical mechanism

To illustrate how summer cold SST anomalies in the North Atlantic result in a stronger EAWM, cold-minus-warm composite maps of geopotential height at 700-hPa on the Northern Hemisphere from July(-1) to April(0) are shown in Fig. 8. The left column of Fig. 8 shows that two centers with significantly positive geopotential height anomalies are located near England/Denmark and near Lake Baikal. The positive geopotential height near Lake Baikal indicates that the Siberian high is enhanced from October(-1) to April(0), and thus the EAWM is strengthened, agreeing with the results of Fig. 7. On the other hand, geopotential height anomalies exhibit two negative centers over the North Atlantic and north or northeast of the Caspian Sea.

The East Atlantic/West Russia (EA/WR) teleconnection pattern (Barnston and Livezey 1987) is shown in the right column of Fig. 8. To some degrees, cold-minus-warm composite patterns of the geopotential height anomalies at 700-hPa

(the left column of Fig. 8) are similar to the EA/WR teleconnection patterns. The pattern correlation coefficients, which measure the spatial correlations between the left and right column fields, are 0.51, 0.63, 0.54, and 0.36 with a sample size up to a total number of grids north of 20ºN (all exceeding the 95% confidence level). In addition, correlation between the monthly NAI and the EA/WR index from 1950-2003 is -0.17 exceeding the 95% confidence level, suggesting that North Atlantic SST anomalies are associated with the EA/WR teleconnection. The EA/WR teleconnection is also associated with zonal wind anomalies over the tropical Pacific. The EA/WR teleconnection shows significant correlation with low-level zonal wind anomalies over the western and central tropical Pacific, especially in the boreal winter and spring (Fig. 9). When the EA/WR teleconnection is on positive phase in DJF and MAM, low-level westerlies tend to develop over the western and central tropical Pacific. The correlation patterns between the EA/WR teleconnection and zonal wind anomalies over the tropical Pacific in DJF and MAM (Fig. 9c and 9d) are similar to cold-minus-warm composite difference patterns in Figs. 4c and 4d, indicating the important role of the EA/WR teleconnection connecting northern Atlantic SST anomalies and westerlies over the western tropical Pacific. Therefore, it is possible that the impact of cold North Atlantic SST anomalies on East Asia is conveyed through Eurasia via the EA/WR teleconnection pattern. The teleconnected effect is to strengthen the intensity of the Siberian high during July(-1) to April(0), leading to the stronger EAWM over East Asia. The stronger EAWM excites westerly wind over the western tropical Pacific, and thus initiates El Niño.

The centers of the EA/WR teleconnetion pattern are associated with the planetary Rossby wave energy propagation. Since mid-latitude westerlies act as a Rossby waveguide (Hoskins and Ambrizzi, 1993), the wave energy propagates along the westerlies eastward to East Asia. This process can be properly presented by examining the wave activity flux, which is useful to identify the three-dimensional propagation and source of stationary wave activity (Plumb, 1985). In this study, the wave activity flux evaluated from composite of the cold summer NAI years is analyzed during July(-1) to April(0). The wave activity flux, F_s, is given as (Plumb, 1985):

$$F_s = p\cos\phi \times \begin{pmatrix} v'^2 - \dfrac{1}{2\Omega a \sin 2\phi}\dfrac{\partial(v'\Phi')}{\partial\lambda} \\ -u'v' + \dfrac{1}{2\Omega a \sin 2\phi}\dfrac{\partial(u'\Phi')}{\partial\lambda} \\ \dfrac{2\Omega\sin\phi}{S}\left[v'T' - \dfrac{1}{2\Omega a\sin 2\phi}\dfrac{\partial(T'\Phi')}{\partial\lambda}\right] \end{pmatrix}$$

where $S = \dfrac{\partial\hat{T}}{\partial z} + \dfrac{\kappa\hat{T}}{H}$ is the static stability; the caret indicates an areal average over the area north of 20ºN; p is the pressure; a is the radius of the earth; ϕ and λ are latitude and longitude; Φ is geopotential height and Ω is the Earth's rotation rate. The prime denotes deviation from the zonal mean.

Figure 10 shows horizontal wave activities at 700-hPa from July(-1) to April(0). Two wavetrains spreading eastward across the North Atlantic and the mid-latitude region of East Asia (60º-150ºE) are seen in October(-1), January(0) and April(0). The wavetrain also appears over the eastern North Pacific and western North America in

October(-1) and January(0). In the mid-latitude of the North Atlantic west of 30ºW, the wave flux has a clear divergent component (Figs. 10b, 10c and 10d), suggesting that this region is one of source regions for wave activity. It is well known that the wave activity flux divergence and convergence indicate dissipation and accumulation of wave energy, which may contribute to the formation of cyclonic and anticyclonic circulations. Many studies indicated that a convergent wave activity flux associated with an incoming stationary Rossby wavetrain is of primary importance in the formation of a blocking anticyclone (e.g., Nakamura 1994; Nakamura et al. 1997). Our Fig. 10 shows a southeastward wave activity flux over the North Atlantic from October(-1) to April(0). This flux is divergent in the western North Atlantic and thus can form a negative geopotential height anomaly centre as shown in Figs. 8b, 8c and 8d. Figure 10 also shows that the eastward wave activity flux is convergent over northeastern Asia, especially over the region around Lake Baikal, and thus enhances the positive geopotential height anomalies over the Siberian, as shown in Figs. 8b, 8c and 8d.

A latitude-height cross-section at 30ºW shows vertical propagating of the anomalous wave energy (Fig. 11). In July(-1), wave activity propagates downward over the North Atlantic (40º-60ºN) at a lower level, whereas wave activity propagates upward from 30º-40ºN (Fig. 11a). In the following months especially in October(-1) to January(0), the anomalous wave energy propagates upward into 200-hPa around the North Atlantic, indicating the conversion of the available potential energy from the mean flow to the disturbances (Figs .11b, 11c and 11d). Given that stationary

planetary waves in the troposphere are forced by the topographic and diabatic heating (Plumb, 1985), SST changes in the North Atlantic may be responsible for the overlying atmospheric anomalous circulations.

The dynamical mechanism linking North Atlantic SST anomalies and atmospheric circulation over Siberia can be summarized as follows. In response to cold North Atlantic SST anomalies, a local atmospheric cyclonic anomaly is formed. In turn, the planetary stationary waves with two distinct wavetrains develop across the North Atlantic, extending over the northeastern Asia from October(-1) to April(0). The wave activity flux is converged over the region around Lake Baikal, and the anticyclonic circulation anomaly is superimposed on the climatological condition over the Siberian region, which enhances the Siberian high. The strengthened Siberian high then enhances the EAWM and affects equatorial wind in the western Pacific and then El Niño.

6. Summary and discussion

a. Summary

The present paper uses observational data to investigate possible influences of North Atlantic SST anomalies on tropical Pacific SST anomalies. It is found that the influence depends on the season. North Atlantic SST anomalies in the boreal summer and winter are negatively related to central-eastern tropical Pacific SST anomalies during the subsequent 5-13 months. In particular, if the North Atlantic is cold in the summer, an El Niño event tends to be initiated in the subsequent spring and summer.

This study also identifies a physical mechanism whereby cold summer North Atlantic SST anomalies influence the El Niño onset in the ensuing year. Composite calculations show that summer cold North Atlantic SST anomalies induce the atmospheric circulation pattern in the Northern Hemisphere that resembles the positive EA/WR teleconnection pattern. Through this teleconnection, the Siberian high enhances and the EAWM strengthens. These are associated with an off-equatorial cyclone in the western Pacific in the subsequent spring which causes equatorial westerly wind anomalies over the western Pacific acting to trigger an El Niño.

The EA/WR teleconnection pattern is related to the planetary Rossby wave energy propagation. When North Atlantic SST is anomalously cold from July(-1) to April(0), the wavetrain forced by SST-induced heating over the midlatitude Atlantic appears in October(-1), and persists to April (0). The wave activity flux over the North Atlantic is divergent, and a negative geopotential height anomaly centre forms over there at the low-level troposphere. Because the westerlies at the mid-latitude act as a waveguide, the wavetrain associated with cold North Atlantic SST anomalies develops over northeastern Asia from October(-1) to April(0). The convergence of eastward wave activity flux east of Lake Baikal generates positive geopotential height anomalies and the Siberian high is thus intensified. Since the Siberian high is strengthened from October(-1) to April(0), and the northerlies over East Asia are enhanced. The anomalous northerlies can bring cold and dry advection from the Asian continent to the western tropical Pacific. The process is associated with the ENSO

western Pacific anomaly pattern with an off-equatorial cyclonic circulation in the western Pacific (Weisberg and Wang 1997b; Wang et al. 1999; Wang and Weisberg 2000). The off-equatorial cyclone induces equatorial westerly winds in the western tropical Pacific, which is in favor of an El Niño onset.

It is noted that Indian Ocean variability can also influence zonal wind anomalies over the western Pacific (e.g., Kug et al. 2005; Kug and Kang 2006; Xie et al. 2002; Misra 2004; Annamalai et al. 2005; Xie et al. 2009). These previous studies have shown that a cooling (warming) in the Indian Ocean tends to be co-varied with westerly (easterly) wind anomalies over the western Pacific through the Walker circulation changes, and thus impacts ENSO variability. The relative roles of North Atlantic and tropical Indian Ocean SST anomalies in the generation of zonal wind anomalies in the western Pacific need to be further studied.

b. Discussion

When North Atlantic SST anomalies are cold in the summer, an El Niño onset tends to occur in the subsequent year in the tropical Pacific. However, we have to keep in mind that this does not always happen. For example, the summer NAI in 1968, 1974, and 1982 is colder than that in the other year, but El Niño does not appear in the these subsequent years. This indicates that an El Niño onset is also influenced by other factors such local ocean-atmosphere interaction processes in the tropical Pacific.

Our analyses have shown that the EAWM is a key factor linking cold North Atlantic SST and the El Niño onset. Although interannual variability of the EAWM

depends largely on variability of the Siberian high, the Aleutian low is another climate factor critically impacting the EAWM (Jhun and Lee 2004, Zhou et al. 2007). However, Figure 8 shows that there are no significant geopotential height anomalies over the mid-latitude North Pacific except for April(0), indicating that variations of the Aleutian low are independent of the teleconnection induced by North Atlantic SST anomalies. Figure 12 confirms this by showing that the boreal summer NAI relates poorly to the following Aleutian low.

To illustrate the influence of the Aleutian low, geopotential height composites of El Niño minus no El Niño during the preceding summer NAI are shown in Figure 13. Except in February(0) and May(0), the signals are not significant around the Siberian region, indicating that the differences of the Siberian high are not evident. However, significant geopotential height anomalies appear over the North Pacific. The centre of positive anomalies is located over the eastern North Pacific in December(-1), and then shifts eastward in January(0). The negative anomalies over the North Pacific are significant and persist from February(0) to May(0), indicating that the Aleutian low is stronger in the El Niño year than that without El Niño. That is to say, when the preceding summer NAI is cold, an El Niño tends to occur in the next spring if the Aleutian low in the winter and next spring is stronger. Therefore, in view of the impact of the Aleutian low on the northerlies over East Asia, the Aleutian low may modulate the influences of cold summer North Atlantic SST anomalies on El Niño onset. This issue will be pursued in future research.

References

Annamalai H, Xie S-P, McCreary JP, Murtugudde R (2005) Impact of Indian Ocean sea surface temperature on developing El Niño. J Clim 18: 302-319

Barnett TP (1983) Interaction of the monsoon and Pacific trade wind system at inter-annual time scales. Part I: The equatorial zone. Mon Wea Rev 111: 756-773

Barnston AG, Livezey RE (1987) Classification, seasonality and persistence of low-frequency atmospheric circulation patterns. Mon Wea Rev 115: 1083-1126

Chu P-S (1988) Extratropical forcing and the burst of equatorial westerlies in the western Pacific: a synoptic study. J Meteorol Soc Jpn 66: 549-564

Chu P-S, Frederick J (1990) Westerly wind bursts and surface heat fluxes in the equatorial western Pacific in May 1982. J Meteorol Soc Jpn 68: 523- 537

Clarke AJ, Shu L (2000) Quasi-biennial winds in the far western equatorial Pacific phase-Locking El Niño to the seasonal cycle. Geophys Res Lett 27(6): 771-774

Clarke AJ, Van Gorder S (2001) ENSO prediction using an ENSO trigger and a proxy for western equatorial Pacific warm pool movement. Geophys Res Lett 28: 579-582

Czaja A, Frankignoul C (2002) Observed impact of Atlantic SST anomalies on the North Atlantic Oscillation. J Clim 15: 606-623

Dong BW, Sutton RT (2002) Adjustment of the coupled ocean-atmosphere system to a sudden change in the Thermohaline Circulation. Geophys Res Lett 29(15): 1728. doi: 10.1029/2002GL015229

Dong BW, Sutton RT, Scaife AS (2006) Multidecadal modulation of El

Niño-Southern Oscillation (ENSO) variance by Atlantic Ocean sea surface temperatures. Geophys Res Lett 33: L08705. doi: 10.1029/2006GL025766

Dong BW, Sutton RT (2007) Enhancement of ENSO variability by a weakened Atlantic Thermohaline circulation in a coupled GCM. J Clim 20: 4920-4939

Enfield D, Mestas-Nunez A, Trimble P (2001) The Atlantic multidecadal oscillation and its relation to rainfall and river flows in the continental U.S. Geophys Res Lett 28: 2077-2080

Gong D-Y, Wang S-W, Zhu J-H (2001) East Asian winter monsoon and Arctic Oscillation. Geophys Res Lett 28(10): 2073-2076

Hoskins BJ, Ambrizzi T (1993) Rossby wave propagation on a realistic longitudinally varying flow. J Atmos Sci 38: 1179-1196

Huang R, Zang X, Zhang R, Chen J (1998) The westerly anomalies over the tropical pacific and their dynamical effect on the enso cycles during 1980-1994. Adv Atmos Sci 15: 135-151

Jhun J-G, Lee E-J (2004) A new East Asian Winter Monsoon index and associated characteristics of the winter monsoon. J Clim 17: 711-726

Knight JR, Folland CK, Scaife AA (2006) Climate impacts of the Atlantic Multidecadal Oscillation. Geophys Res Lett 33: L17706. doi:10.1029/2006GL026242.

Kug J-S, An S-II, Jin F-F, Kang I-S (2005) Preconditions for El Niño and La Niña onsets and their relation to the Indian Ocean. Geophys Res Lett 32: L05706. doi:10.1029/2004GL021674

Kug J-S, Kang I-S (2006) Interactive feedback between ENSO and the Indian Ocean. J Clim 19: 1784-1800

Kushnir Y (1994) Interdecadal variations North Atlantic sea surface temperature and associated atmospheric conditions. J Clim 7: 141-157

Latif M, Arpe K, Roeckner E (2000) Oceanic control of decadal North Atlantic sea level pressure variability in winter. Geophys Res Lett 27: 727-730

Li C (1990) Interaction between anomalous winter monsoon in East Asia and El Niño events. Adv Atmos Sci 7: 36-46

Li C (1995) Westerly anomalies over the equatorial western Pacific and Asian winter monsoon. Proceeding of International Scientific Conference on the TOGA Programme. WCRP-91-WMO/TP, 717: 557-561

Li C, Pei S, Pu Y (2005) Dynamical impact of anomalous East-Asian winter monsoon on zonal wind over the equatorial western Pacific. Chin Sci Bull 50, 1520-1526.

Li Y, Lu R, Dong BW (2007) The ENSO–Asian Monsoon Interaction in a Coupled Ocean–Atmosphere GCM. J Clim 20: 5164-5177

Lu R, Li Y, Dong BW (2007) Arctic Oscillation and Antarctic Oscillation in Internal Atmospheric Variability with an Ensemble AGCM Simulation. Adv Atmos Sci 24: 152-192

Luther D, Harrison D, Knox R (1983) Zonal wind in the central equatorial Pacific and El Niño. Science 202: 327-330

Mann M, Park J (1994) Global-scale modes of surface temperature variability on interannual to century timescales. J Geophys Res 99: 25819–25833

McPhaden MJ (1999) Genesis and evolution of the 1997– 98 El Niño. Science 283: 950-954

Misra V (2004) The teleconnection between the western Indian and the western Pacific ocean. Mon Wea Rev 132: 445-455

Nakamura H (1994) Rotational evolution of potential vorticity associated with a strong blocking flow configuration over Europe. Geophys Res Lett 21: 2003-2006

Nakamura H, Nakamura M, Anderson JL (1997) The role of high- and low-frequency dynamics in the blocking formation. Mon Wea Rev 125: 2074-2093

Nakamura T, Tachibana Y, Honda M, Yamane S (2006) Influence of the Northern Hemisphere annular mode on ENSO by modulating westerly wind bursts. Geophys Res Lett 33: L07709. doi: 10.1029/2005GL025432

Philander SG (1985) El Niño and La Niña. J Atmos Sci 42: 2652- 2662

Plumb RA (1985) On the three-dimensional propagation of stationary waves. J Atmos Sci 42: 217- 229

Rasmusson EM, Carpenter TH (1982) Variations in tropical sea surface temperature and surface wind fields associated with the Southern Oscillation/El Niño. Mon Wea Rev 110: 354-384

Rayner NA, Parker DE, Horton EB, Folland CK, Alexander LV, Rowell DP, Kent EC, Kaplan A (2003) Global analyses of sea surface temperature, sea ice, and night marine air temperature since the late nineteenth century. J Geophys Res 108: 4407. doi: 10.1029/2002JD002670

Rodwell MJ, Rowell DP, Folland CK (1999) Oceanic forcing of the wintertime North Atlantic Oscillation and European climate. Nature 398: 320-323

Sutton RT, Hodson DLR (2007) Climate response to Basine-Scale warming and cooling of the north Atlantic Ocean. J Clim 20: 891-907

Thompson DWJ, Lorenz DJ (2004) The signature of the annular modes in the tropical troposphere. J Clim 17: 4330-4342

Timmermann A, An S-I, Krebs U, Goosse H (2005) ENSO suppression due to weakening of the North Atlantic Thermohaline Circulation. J Clim 18: 3122-3139.

Trenberth KE, Hurrell JW (1994) Decadal atmosphere-ocean variations in the Pacific. Clim Dyn 9: 303–319

Trenberth KE (1997) The definition of El Niño. Bull Amer Meteor Soc 78: 2771-2777

Wallace JM, Gutzler DS (1981) Teleconnections in the geopotential height field during the Northern Hemisphere winter. Mon Wea Rev 109: 784-812

Wang B, Wu R, Fu X (2000) Pacific–East Asian teleconnection: How does ENSO affect East Asian climate? J Clim 13: 1517-1536

Wang B, An S-I (2002) A mechanism for decadal changes of ENSO behavior: Roles of background wind changes. Clim Dyn 18: 475-486

Wang B, Zhang Q (2002) Pacific–East Asian teleconnection. Part II: How the Philippine Sea anomalous anticyclone is established during El Niño development. J Clim 15: 3252-3265

Wang C, Weisberg RH, Virmani J (1999) Western Pacific interannual variability

associated with the El Niño-Southern Oscillation. J Geophys Res 104: 5131-5149

Wang C, Weisberg RH (2000) The 1997-98 El Niño evolution relative to previous El Niño events. J Clim 13: 488-501.

Wang D, Wang C, Yang X, Lu J (2005) Winter Northern Hemisphere surface air temperature variability associated with the Arctic Oscillation and North Atlantic Oscillation. Geophys Res Lett 32: L16706. doi:10.1029/2005GL022952

Wang X, Wang D, Zhou W (2009) Decadal variability of twentieth- century El Niño and La Niña occurrence from observations and IPCC AR4 coupled models, Geophys Res Lett 36: L11701. doi:10.1029/2009GL037929

Weisberg RH, Wang C (1997a) Slow variability in the equatorial west-central Pacific in relation to ENSO. J Clim 10: 1998-2017

Weisberg RH, Wang C (1997b) A western Pacific oscillator paradigm for the El Niño-Southern Oscillation. Geophys Res Lett 24: 779-782

Wu BY, Wang J (2002) Possible impacts of winter Arctic Oscillation on Siberian high, the East Asian winter monsoon and sea-ice extent. Adv Atmos Sci 19: 297–320

Wyrtki K (1975) El Niño-the dynamic response of the equatorial Pacific Ocean to atmospheric forcing. J Phys Oceanogr 5: 572-584

Xie S-P, Annamanlai H, Schott FA, McCreary JP (2002) Structure and mechanisms of south Indian Ocean climate variability. J Clim 15: 864-878

Xie S-P, Hu K, Hafner J, Tokinaga H, Du Y, Huang G, Sampe Y (2009) Indian Ocean capacitor effect on Indo-western Pacific climate during the summer following El

Niño. J Clim 22: 730-747

Xu J, Chan JCL (2001) The role of the Asian/Australian monsoon system in the onset time of El Niño events. J Clim 14: 418-433

Zhou W, Li C, Wang X (2007) Possible connection between Pacific Oceanic interdecadal pathway and east Asian winter monsoon. Geophys Res Lett 34: L01701. doi:10.1029/2006GL027809

Zhang R, Delworth TL (2005) Simulated tropical response to a substantial weakening of the Atlantic Thermohaline Circulation. J Clim 18: 1853-1860

List of Tables and Figures

Table 1. Years prior to El Niño and La Niña years during 1958-2001. In El Niño (-1) and La Niña (-1) year, the bold years represent the years when the summer (June-August) North Atlantic is cold and warm (the NAI exceed ±0.5 standard deviation), respectively. The study is focused on the period of 1958-2001 because the atmospheric reanalysis field is used during this period.

Figure 1. Lagged correlation coefficients between the NAI and Nino-3.4 index during 1870-2003. The X-axis denotes months by which the Nino-3.4 index is lagged the NAI. The shading represents the correlation exceeding the 95% confidence level.

Figure 2. Lagged correlation coefficients between the summer NAI and the SST anomalies during 1870-2001 in (a) concurrent July and subsequent (b) October, (c) January and (d) April. Only exceeding the 95% confidence level are plotted.

Figure 3. Same as Figure 2, except for the zonal wind at 10m during 1958-2001.

Figure 4. Composite differences of the zonal wind at 850-hPa between the cold and warm summer NAI for (a) July (-1), (b) October (-1), (c) January (0) and (d) April (0), respectively. Red (Blue) shading denotes regions of difference at 95% confidence level with a positive (negative) value of zonal wind. As in Rasmusson and Carpenter (1982), month prior to the El Niño year and month in the El Niño year are referred to

month(-1) and month(0), respectively.

Figure 5. Same as Figure 4, except for wind fields at 850-hPa.

Figure 6. Same as Figure 4, except for zonal wind at 200-hPa.

Figure 7. Same as Figure 4, except for SLP.

Figure 8. The left column is the composite difference of the geopotential height at 700-hPa between the cold and warm summer NAI in (a) July(-1), (b) October(-1), (c) January(0) and (d) April(0). The right column is the linear regression coefficients between the geopotential height at 700-hPa and the EA/WR index. Shading denotes regions of difference at 95% confidence level.

Figure 9 Linear correlation coefficients between grid-point zonal wind at 850-hPa and the EA/WR index. Shading denotes regions reaching the 95% confidence level.

Figure 10. The composite wave-activity flux (units: m^2/s^2) for the cold summer NAI at 700-hPa in (a) July(-1), (b)October (-1), (c)January (0) and (d) April(0).

Figure 11. The composite wave-activity flux (units: m^2/s^2) for the cold summer NAI in meridional-vertical section along 30W in (a) July(-1), (b) October(-1), (c)

January(0) and (d) April(0). The vertical component of wave activity flux is arbitrarily enlarged before plotting. The wave-activity flux has been interpolated vertically.

Figure 12. Lagged correlation coefficients between the NAI and North Pacific Index (NPI) during 1899-2003. The X-axis denotes months by which the NPI is lagged the NAI. Shaded areas represent the correlation exceeding the 95% confidence level. The NPI provides a measure of the intensity of the winter Aleutian Low. The NPI is an area-weighted average of the monthly SLP over the region 30–65N, 160E–140W (Trenberth and Hurrell, 1994). The monthly NPI (Jan, 1899–Dec 2003) is available at http://www.cgd.ucar.edu/cas/jhurrell/indices.data.html#npmon.

Figure 13. Composite difference of the geopotential height at 700-hPa between El Niño and no El Niño occurrence for the summer NAI being lower than -0.5 standard deviation in (a) December(-1), (b) January(0), (c) February(0), (d) March(0), (e) April(0), and (f) May(0). Red/Blue shading denotes the regions of difference at 95% confidence level with positive/negative values of the geopotential height.

Table 1. Years prior to El Niño and La Niña years during 1958-2001. In El Niño (-1) and La Niña (-1) year, the bold years represent the years when the summer (June-August) North Atlantic is cold and warm (the NAI exceed ±0.5 standard deviation), respectively. The study is focused on the period of 1958-2001 because the atmospheric reanalysis field is used during this period.

El Niño (-1) year	**1962, 1964**, 1967, **1971**, **1975, 1976**, **1978**, **1981, 1985**, 1990, **1992**, **1993**, and 1996
La Niña (-1) year	1963, 1969, **1972**, 1973, **1983, 1987**, 1994, and **1997**

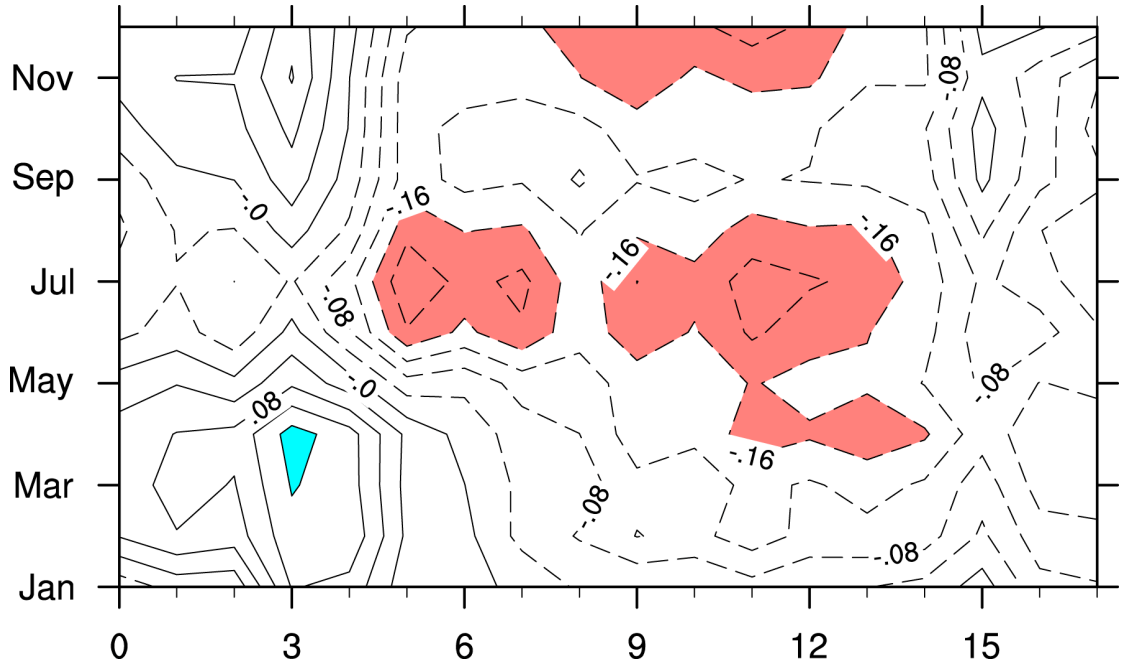

Figure 1. Lagged correlation coefficients between the NAI and Nino-3.4 index during 1870-2003. The X-axis denotes months by which the Nino-3.4 index is lagged the NAI. The shading represents the correlation exceeding the 95% confidence level.

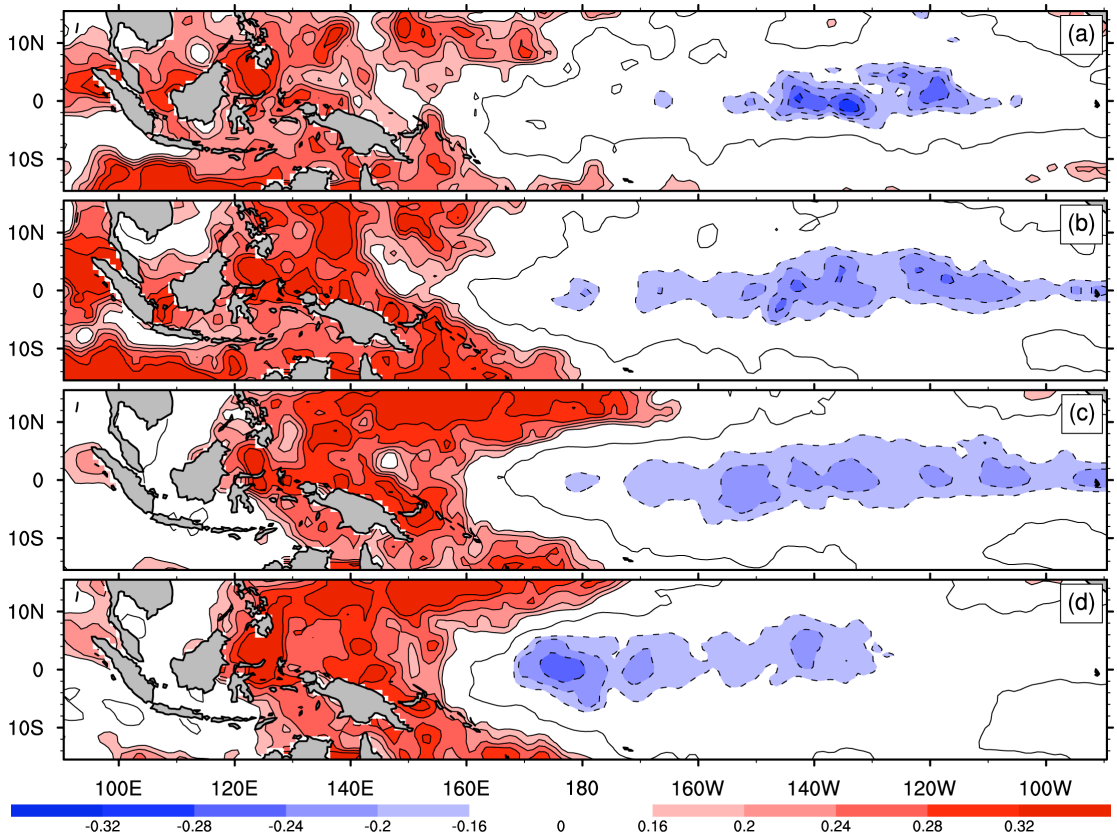

Figure 2. Lagged correlation coefficients between the summer NAI and the SST anomalies during 1870-2001 in (a) concurrent July and subsequent (b) October, (c) January and (d) April. Only exceeding the 95% confidence level are plotted.

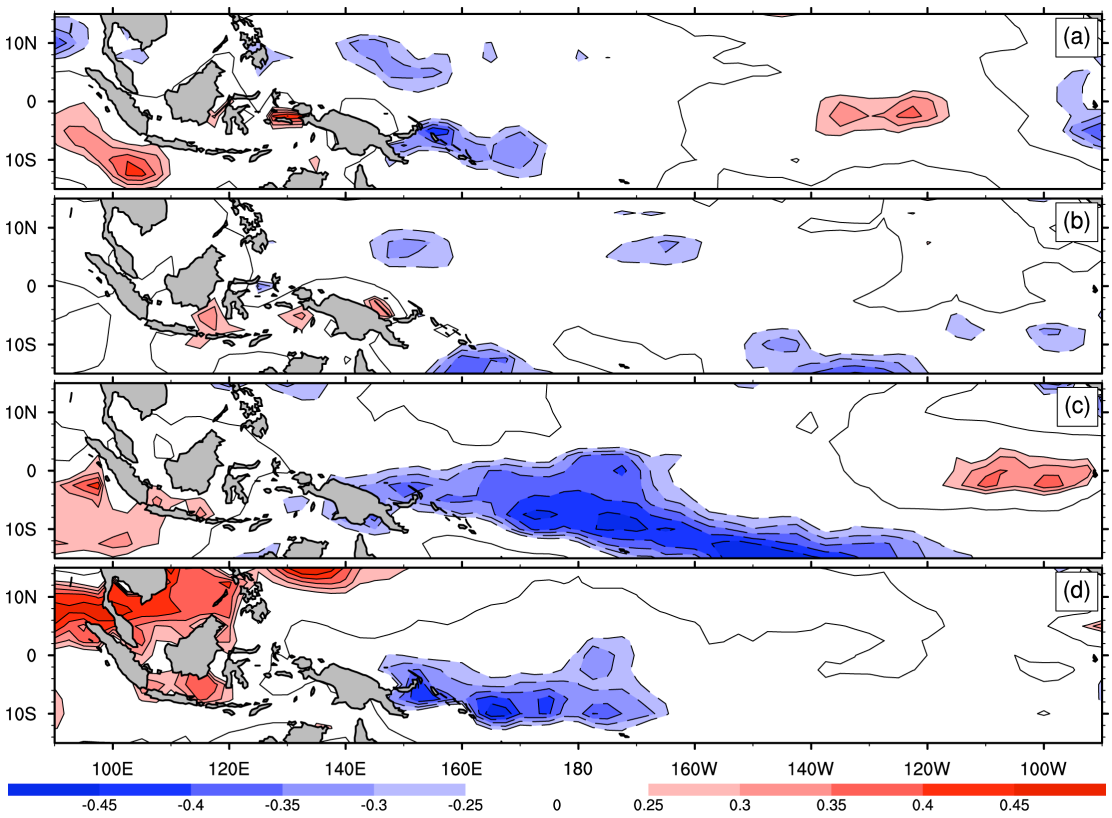

Figure 3. Same as Figure 2, except for the zonal wind at 10m during 1958-2001.

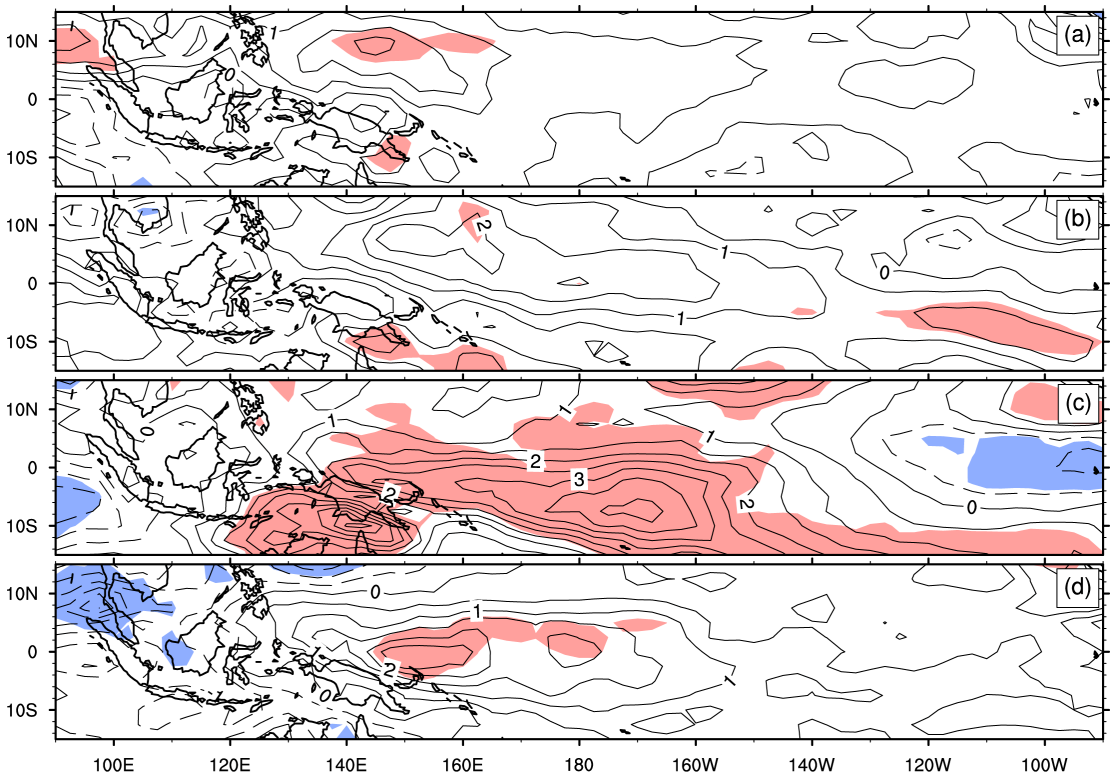

Figure 4. Composite differences of the zonal wind at 850-hPa between the cold and warm summer NAI for (a) July (-1), (b) October (-1), (c) January (0) and (d) April (0), respectively. Red (Blue) shading denotes regions reaching the 95% confidence level with a positive (negative) value of zonal wind. As in Rasmusson and Carpenter (1982), month prior to the El Niño year and month in the El Niño year are referred to month(-1) and month(0), respectively.

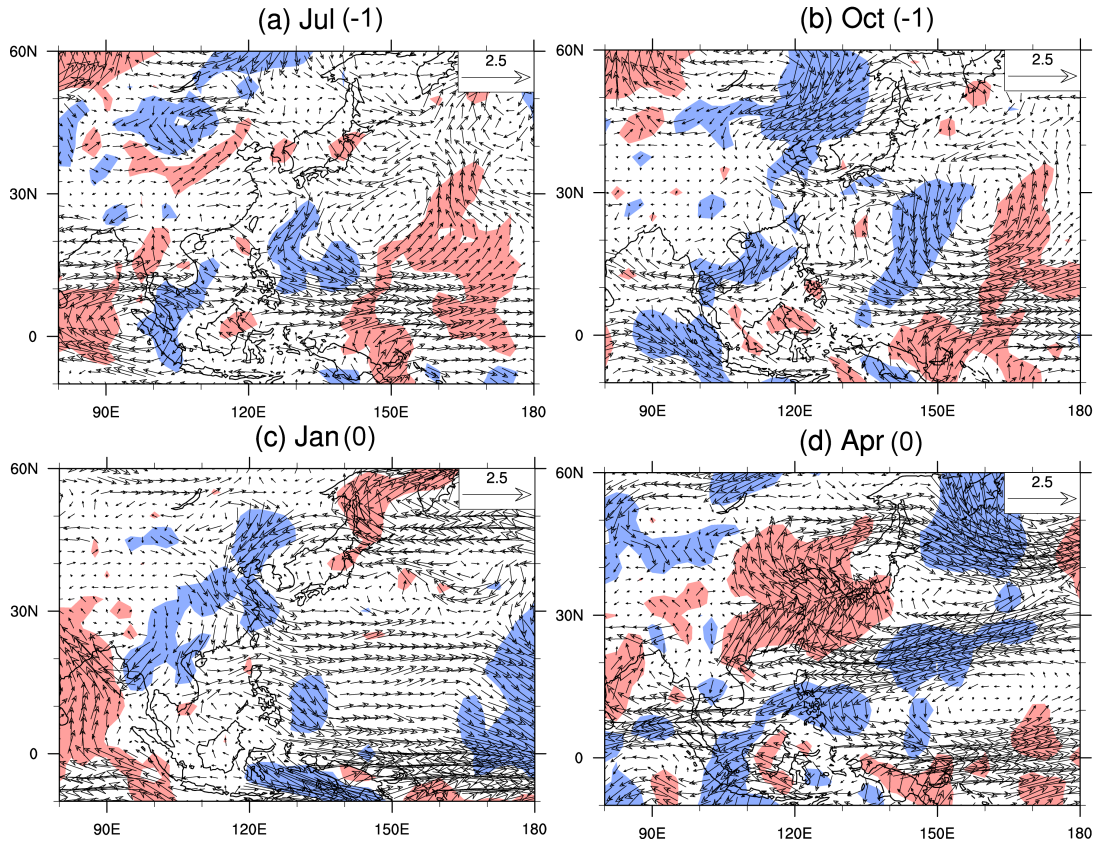

Figure 5. Same as Figure 4, except for wind fields at 850-hPa.

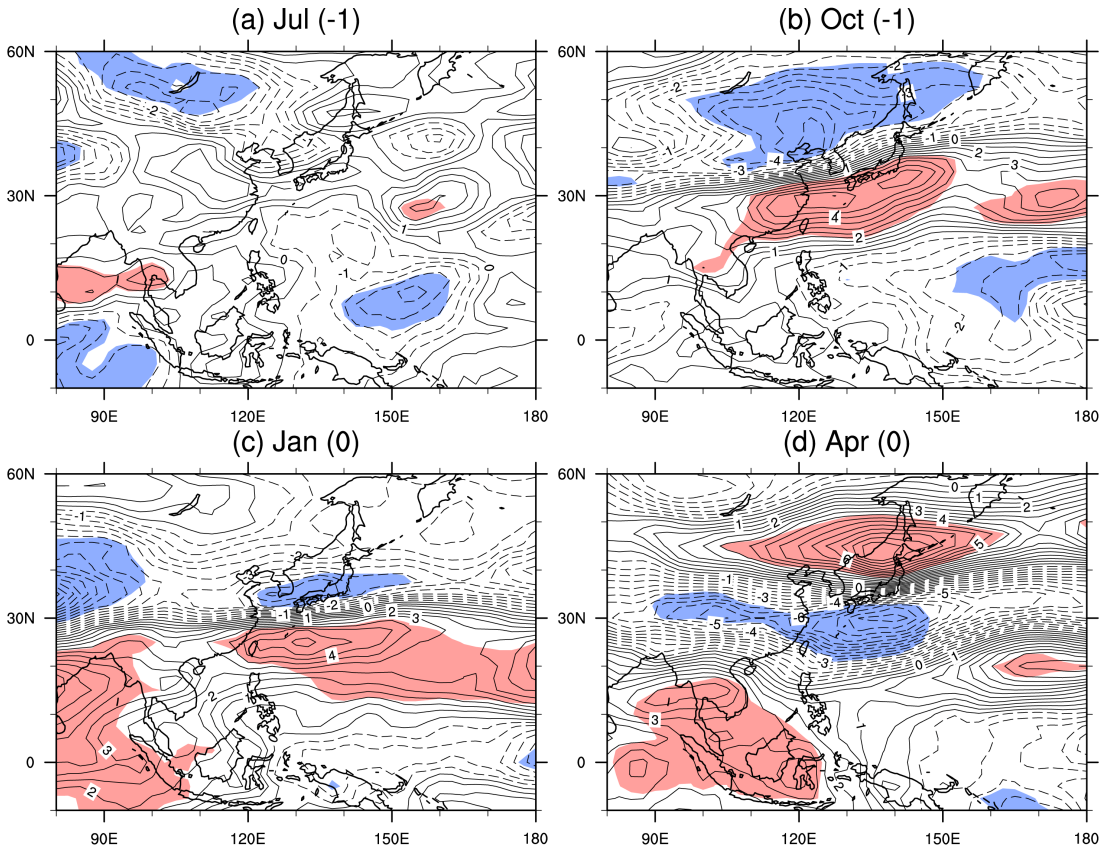

Figure 6. Same as Figure 4, except for zonal wind at 200-hPa.

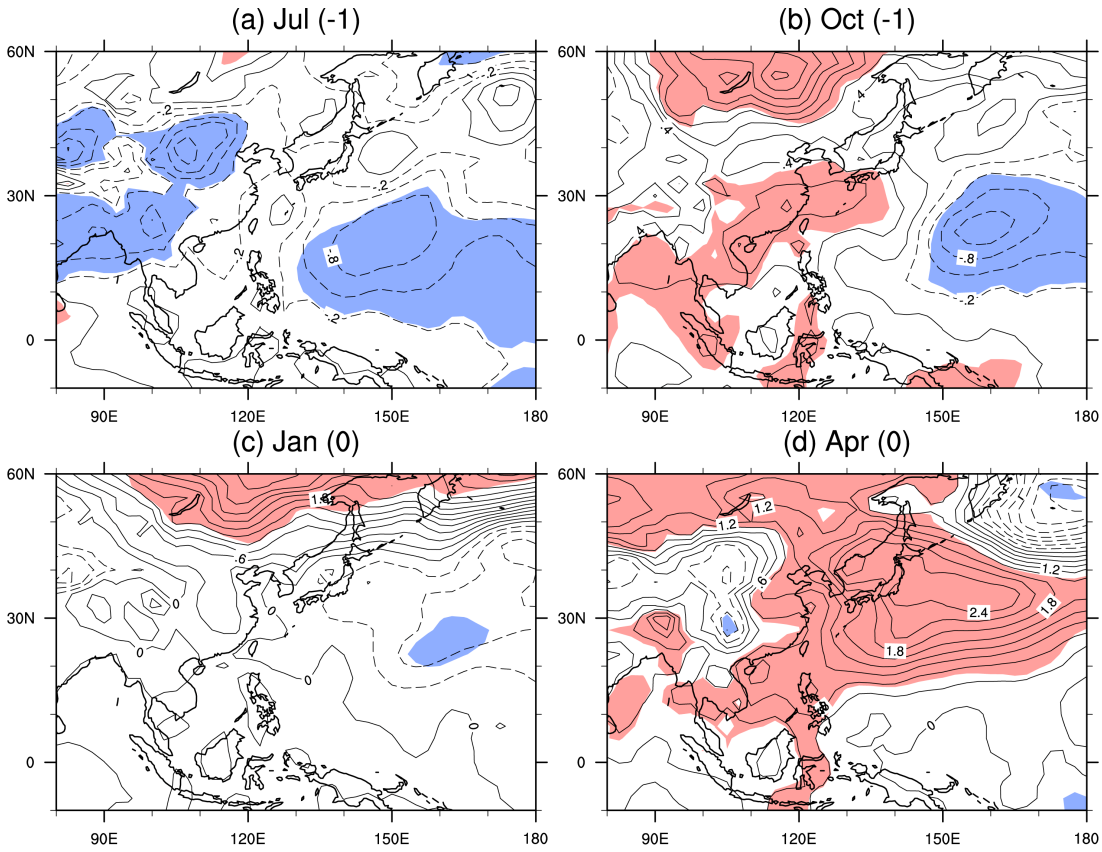

Figure 7. Same as Figure 4, except for SLP.

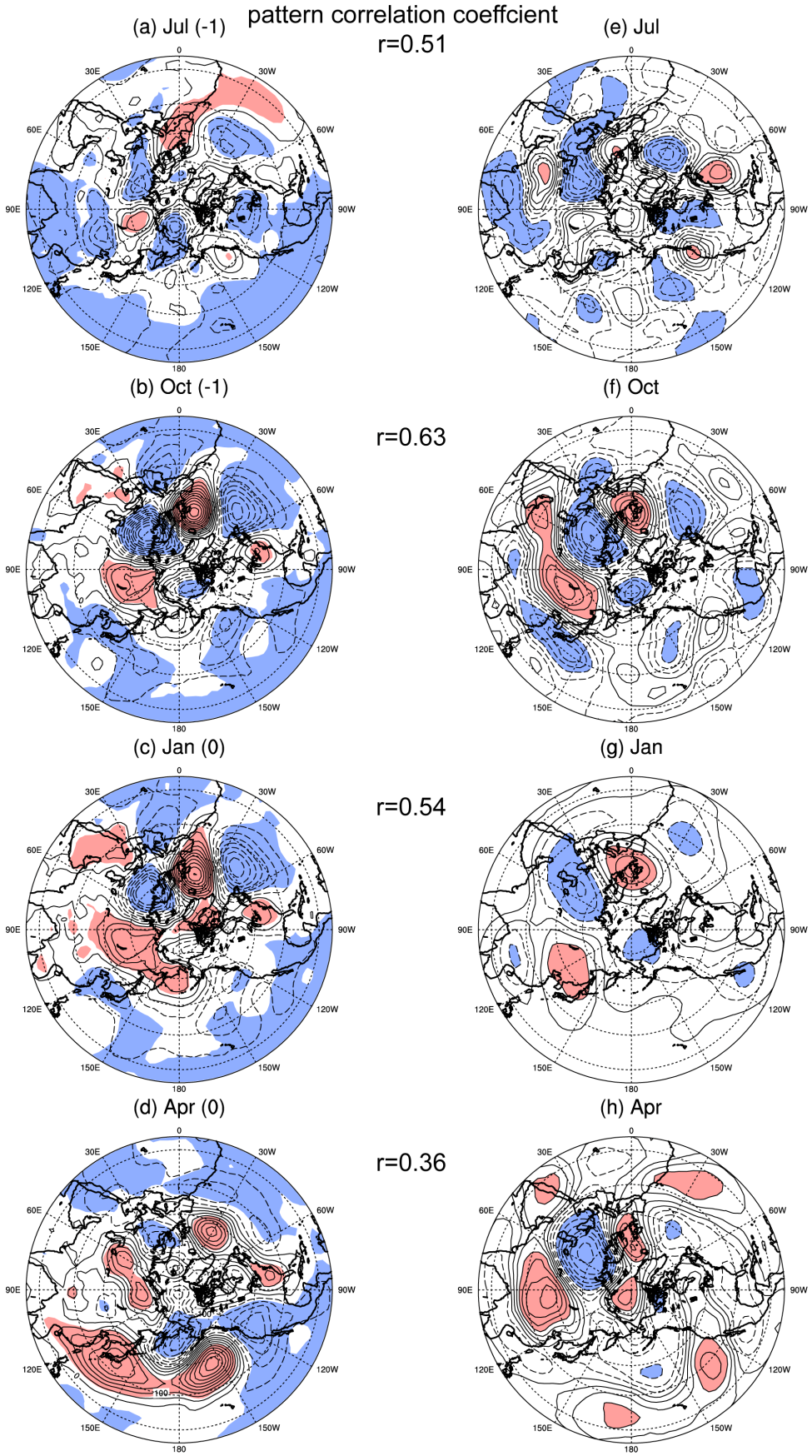

Figure 8. The left column is the composite difference of the geopotential height at

700-hPa between the cold and warm summer NAI in (a) July(-1), (b) October(-1), (c) January(0) and (d) April(0). The right column is the linear regression coefficients between grid-point geopotential height at 700-hPa and the EA/WR index. Shading denotes regions reaching the 95% confidence level.

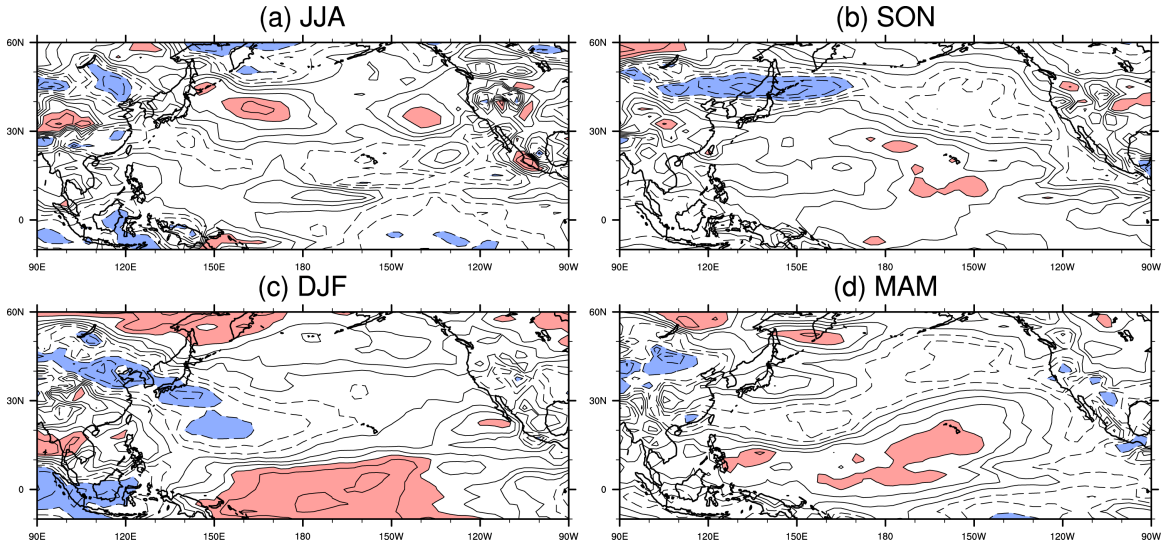

Figure 9. Linear correlation coefficients between grid-point zonal wind at 850-hPa and the EA/WR index. Shading denotes regions reaching the 95% confidence level.

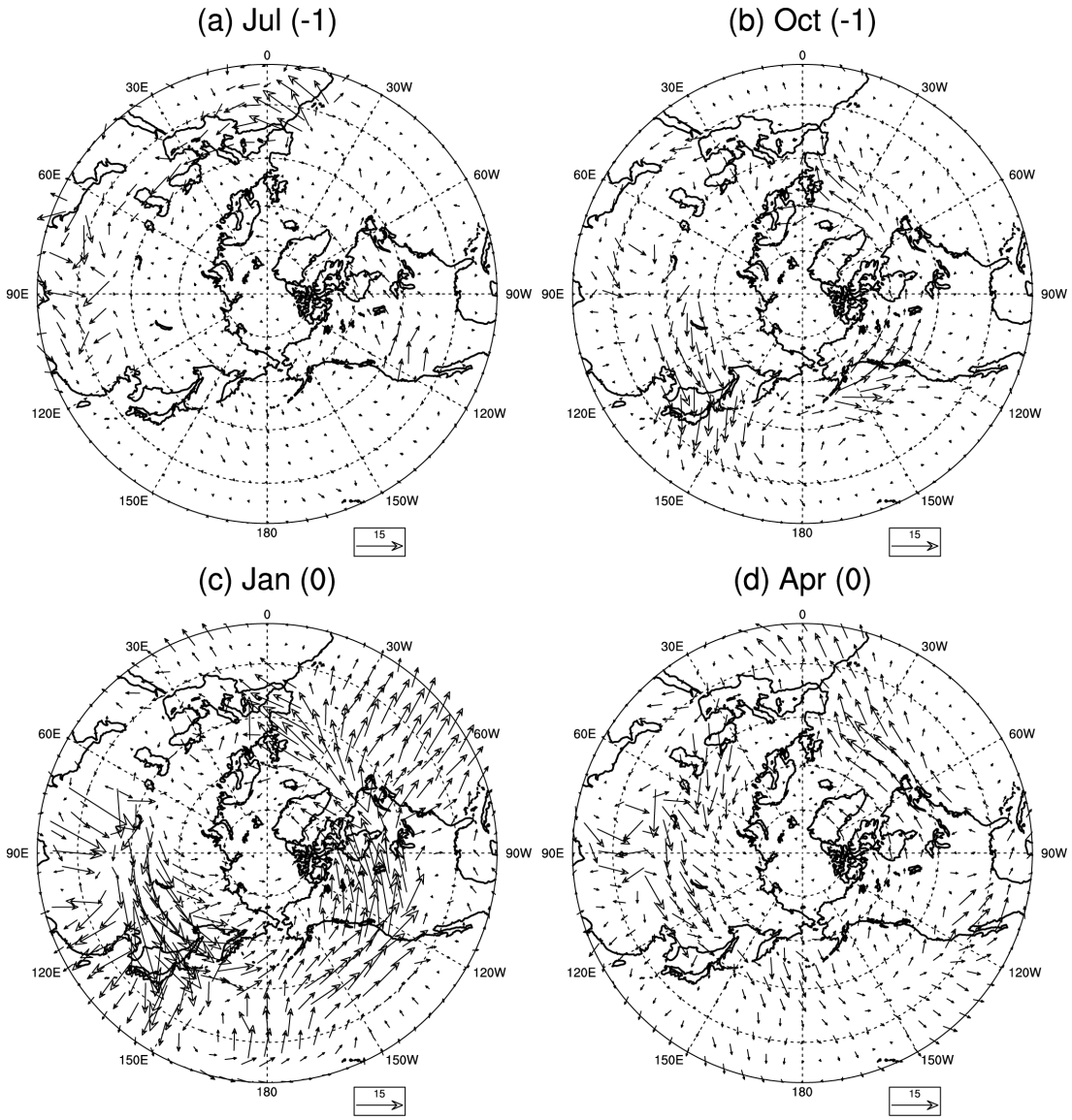

Figure 10. The composite wave-activity flux (units: m^2/s^2) for the cold summer NAI at 700-hPa in (a) July(-1), (b)October (-1), (c)January (0) and (d) April(0).

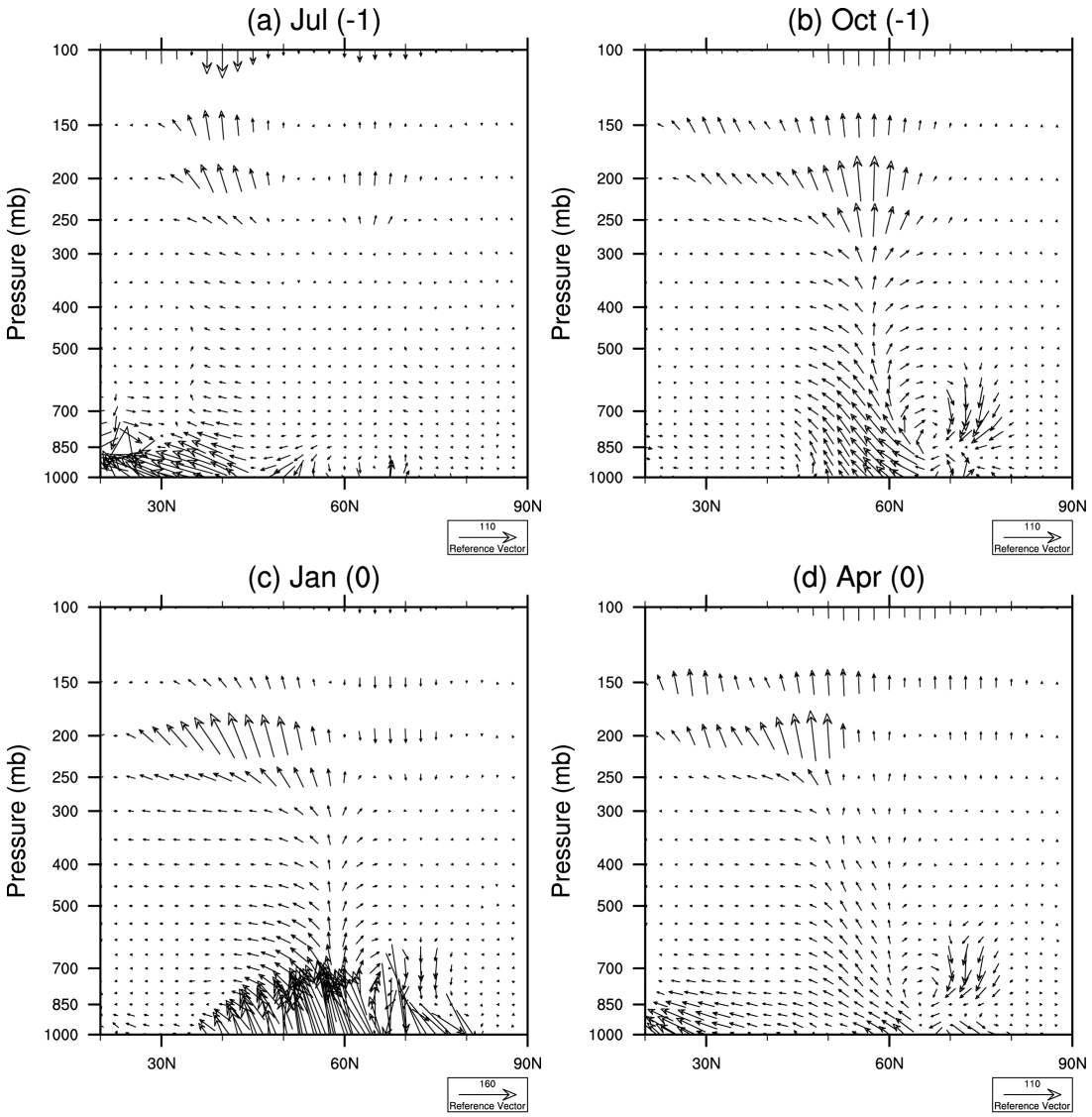

Figure 11. Composite of wave-activity flux (units: m^2/s^2) for the cold summer NAI in meridional-vertical section along 30W in (a) July(-1), (b) October(-1), (c) January(0) and (d) April(0). The vertical component of wave activity flux is arbitrarily enlarged before plotting. The wave-activity flux has been interpolated vertically.

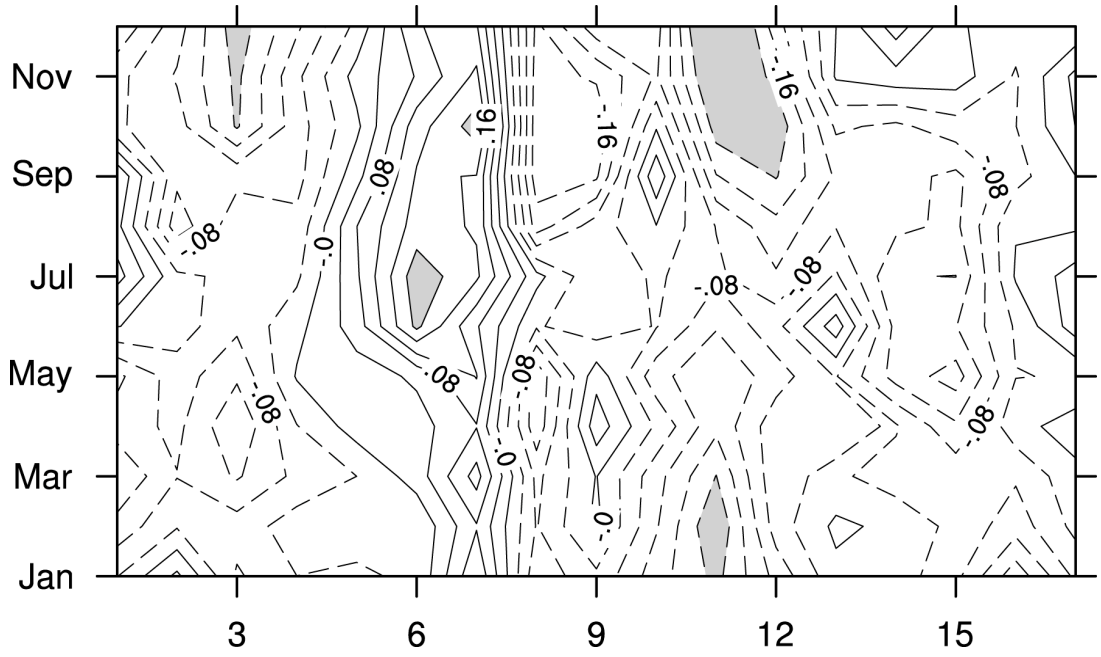

Figure 12. Lagged correlation coefficients between the NAI and North Pacific Index (NPI) during 1899-2003. The X-axis denotes months by which the NPI is lagged the NAI. Shaded areas represent the correlation exceeding the 95% confidence level. The NPI provides a measure of the intensity of the winter Aleutian Low. The NPI is an area-weighted average of the monthly SLP over the region 30–65N, 160E–140W (Trenberth and Hurrell, 1994). The monthly NPI (Jan, 1899–Dec 2003) is available at http://www.cgd.ucar.edu/cas/jhurrell/indices.data.html#npmon.

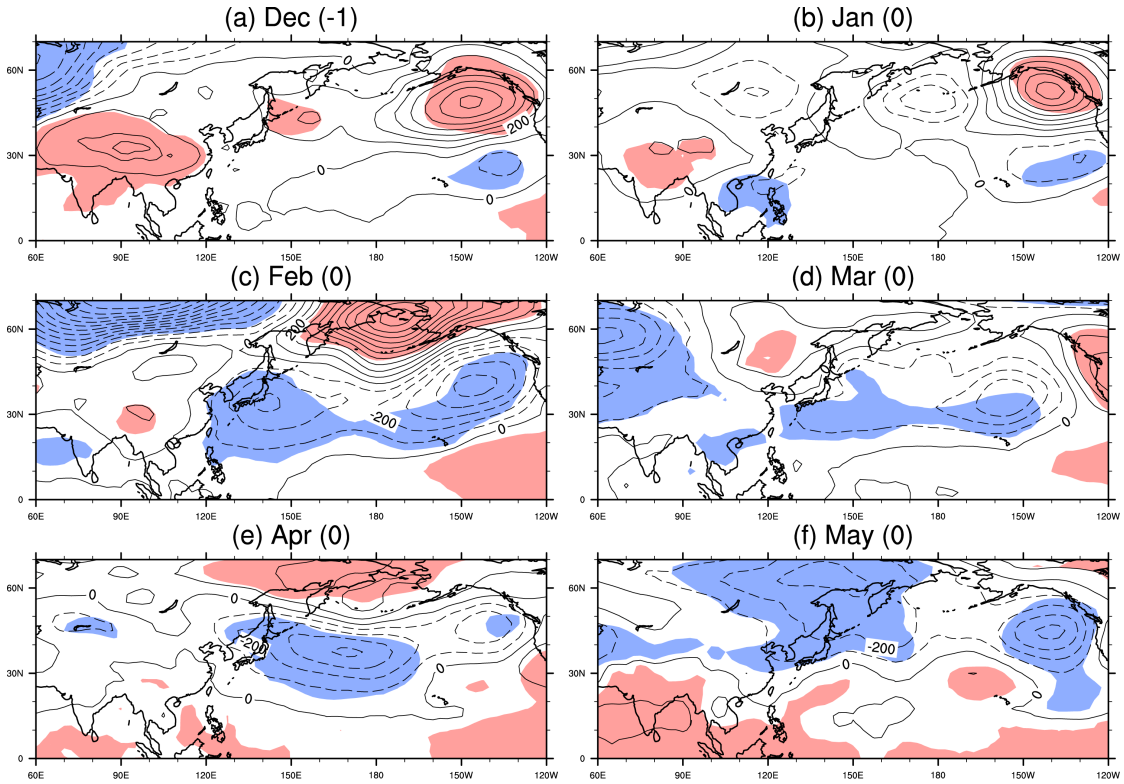

Figure 13. Composite difference of the geopotential height at 700-hPa between El Niño and no El Niño occurrence for the summer with a NAI lower than -0.5 standard deviation in (a) December(-1), (b) January(0), (c) February(0), (d) March(0), (e) April(0), and (f) May(0). Red/Blue shading denotes regions of difference at the 95% confidence level with positive/negative values of the geopotential height.